Acta Geotechnica (2017) 12:1243–1260
DOI 10.1007/s11440-017-0606-5

RESEARCH PAPER

Fracture evolution and energy mechanism of deep-buried carbonaceous slate

Ziquan Chen[1] · Chuan He[1] · Di Wu[1] · Guowen Xu[1] · Wenbo Yang[1]

Received: 16 February 2017 / Accepted: 31 October 2017 / Published online: 10 November 2017

Abstract In order to study the influence of confining pressure and water content on the mechanical properties, fracture evolution and energy damage mechanism of deep-buried carbonaceous slate, uniaxial and triaxial compression tests were carried out under natural and saturated states and acoustic emission monitored. The deep-buried carbonaceous slate samples were obtained at a depth of 1020 m from the Lanjiayan tunnel in Sichuan province, China, where the maximum in situ stress has been measured at 44.2 MPa. The results suggest that water has a significant softening effect on the strength and deformation characteristics of carbonaceous slate, but the effect decreases with an increase in the confining pressure. When both the confining pressure and water content are increased, the acoustic emission events and dissipated energy gradually increase at the pre-peak and post-peak stages. Thus, the AE evolution type seen in the natural state under low confining pressure usually presents as a *main shock*-type event, and it changes to a *foreshock–main shock–after shock* event when saturated and at high confining pressures. Based on the S-shaped energy evolution law, the damage evolution process of carbonaceous slate was analyzed. The damage stress thresholds σ_{ea} and σ_{eb} were obtained, which can be considered as the thresholds of the rock entering the energy-hardening and energy-softening stages. Finally, a new brittleness energy index *BDE* is proposed to describe the influence of confining pressure and water content on the damage mechanism of deep-buried carbonaceous slate.

Keywords Damage evolution · Deep-buried carbonaceous slate · Energy mechanism · Mechanical property

1 Introduction

Carbonaceous slate strata are widely distributed in western China. The basic features of carbonaceous slate include low strength, well-developed joint fissures, and softening due to water infiltration. When a tunnel passes through a carbonaceous slate stratum, the deformation of the surrounding rock is often rapid, large and long-lasting. There is also the likelihood that the tunnel will undergo more large deformations and be more susceptible to collapse, imposing a great impact on the construction and future operation of the tunnel [19, 30]. During the excavation of a deep-buried long tunnel, the surrounding rock is subjected to complicated geological conditions with high geo-stresses and high seepage pressures. The mechanical properties, deformation characteristics, failure mechanism, and energy mechanism of the surrounding rock will be significantly altered under high confining pressure and increased saturation [11, 20, 34, 36].

The influences of high confining pressure and water content on the mechanical properties of rock have been studied by several investigators. Erguler and Ulusay [8] quantified the effects of water content on the mechanical properties of rock and developed a method for estimating the rock strength and deformability at any water content. Yang et al. [35] found that the Young's modulus of red sandstone has a nonlinear relationship with the confining pressure, but the Poisson's ratio remained unaffected. Yu

✉ Ziquan Chen
chen_ziquan@163.com

[1] Key Laboratory of Transportation Tunnel Engineering, Ministry of Education, Southwest Jiaotong University, Chengdu 610031, China

et al. [37] reported that water significantly affects the stress relaxation of silty mudstone, which should not be ignored in the design and construction of major projects. Nara et al. [22, 23] and Nakao et al. [21] concluded that crack growth in various rocks is affected by humidity, which in turn affects the mechanical stability of the rock mass. Tjioe and Borja [28, 29] explained the microfracturing mechanism of crystalline rocks using pore-scale simulations. Using a 3D discrete element method, Duan et al. [6] studied the effect of confine pressure on peak stress, Young's modulus, failure plane angles, the brittle–ductile transition, and the evolution of failure modes. Bennett et al. [2] and Semnani et al. [27] studied the effect of anisotropy in layered rocks.

Based on the progressive fracture characteristic of rock, its deformation and failure processes include initiation, propagation, extension, coalescence of internal cracks, and unstable macroscopic fractures [3, 7, 26, 38]. The acoustic emission (AE) technique can be used to detect the crack evolution process and interior damage of the rock [25, 32]. Based on the energy evolution mechanism, the deformation and failure of the rock can be divided into the processes of energy input, elastic strain energy accumulation, energy dissipation, and energy release. The damage evolution of a rock and its final unstable failure are driven by the energy [5, 12, 33]. The initiation and propagation of cracks lead to the dissipation of energy within the rock; this release of energy is the inherent reason for the rock's sudden failure. Therefore, the fracture evolution process of rock is closely linked with the energy evolution mechanism.

In order to study the damage evolution process in rocks, some macroscopic characteristic variables are often used to classify the degree of damage in a rock, such as the elastic modulus, yield stress, ultrasonic velocity, and CT scanning [9, 15, 24]. The damage evolution and final unstable failure of rock are driven by the energy balance; initiation and propagation of cracks are accompanied by energy dissipation and energy release. In recent years, the study of fracture and damage evolution based on AE characteristics and the energy balance mechanism have been a topic of much research [4, 10, 13, 14]. However, few studies have analyzed the influence of high confining pressure and water content on the mechanical properties of deep-buried carbonaceous slate based on the energy balance mechanism and damage evolution.

In this research, an MTS815 rock mechanics test system and a PCI-II acoustic emission system were used to conduct uniaxial and conventional triaxial compression tests on samples of deep-buried carbonaceous slate. The deep-buried carbonaceous slate samples were retrieved at a depth of 1020 m from the Lanjiayan tunnel in Sichuan province, China, where the measured maximum in situ stress was 44.2 MPa. The influence of high confining pressure and water content on the mechanical properties, fracture evolution, and energy balance mechanism of deep-buried carbonaceous slate are systematically discussed. Based on the energy balance mechanism, the damage evolution in carbonaceous slate under different confining pressures and water contents is analyzed. Finally, the damage stress thresholds σ_{ea} and σ_{eb} were obtained and a new brittleness energy index *BDE* is proposed to describe the influence of confining pressure and water content on the damage evolution mechanism seen in deep-buried carbonaceous slate.

2 Engineering background and experimental plan

2.1 Engineering background of deep-buried carbonaceous slate

In recent years, transportation tunnels, resource exploitation, and diversion tunnels have become a key area in deep underground engineering. With the increases in rock engineering activities at greater depths, the geo-stresses encountered also increase. The mechanical properties and fracture mechanisms in deep-buried soft rock are complicated. The fracture evolution process and damage mechanism during excavation have obvious nonlinear mechanical characteristics, which is quite different to engineering projects at shallow depths. Tunneling projects undertaken in this deep-buried and carbonaceous slate stratum encountered large deformations of the surrounding rock, serious distortion of the steel arch, and significant cracks in the lining (Fig. 1). Based on Table 1, it can be concluded that these deep-buried soft rock tunnels often have high ground stresses and low rock strength characteristics. After the excavation of the tunnel, the supporting structure often experienced intense and persistent squeezing deformations because of the poor self-stabilization capability of the surrounding rock. The specific performance sequence is deformation occurrence, deformation growing, large deformation, support structure cracking, arch twist, and then continuous extrusion. Previous investigations into the behavior of soft rock tunnels indicated that the squeezing pressure and mechanical behavior of the soft rock were the main reasons for the large deformations, and soft rocks have significant aging fracture characteristics under the action of high geo-stresses and excavation disturbance. However, the fracture evolution and damage mechanism of deep-buried soft rocks are not clear at present; soft rocks often have water softening and argillization characteristics due to the high clay content. Accordingly, the long-term deformation and support structure damage are closely related to both aging fractures and the water-softening characteristics of the soft rock.

Fig. 1 Deformation and failure characteristics of typical deep-buried carbonaceous slate tunnel

Table 1 Statistical results of typical deep-buried soft rock tunnels in western China

Tunnel	Depth (m)	σ_1^{max} (MPa)	Compressive strength of rock (MPa)	Maximum deformation (mm)	Deformation/fracture characteristics
Muzhailing railway tunnel	715	27.2	6.9	810	Large deformation under high geo-stress; maximum displacement velocity 20 cm/day
Maoxian railway tunnel	675	27.5	2.0	1200	Large compressive deformation occurred during excavation and lasted for a long time
Gonghe highway tunnel	1000	29.8	11.4	310	The initial support was broken; surrounding rock was under serious bias
Maoyushan railway tunnel	700	21.3	5.6	1712	Fast deformation rate and significant rheological effect; steel arch was badly distorted
Baozhen railway tunnel	630	16.0	3.9	1250	Large asymmetrical deformation occurred during excavation and lasted for a long time
Wushaoling railway tunnel	1100	32.8	2.5	1209	The tunnel passes through a compressive fault and stability of the surrounding rock was poor. Initial deformation rate was fast
Guanjiao railway tunnel	500	22.0	5.0	505	The bottom and sidewall of the trunnel lining showed large compressive deformation with significant destruction
Nibashan highway tunnel	1650	53	25.7	238	Large deformation occurred in the layered soft rock strata; maximum fracture in secondary lining was 5 mm
Tianchiping railway tunnel	1500	26	5	790	Vault settlement did not converge; there were longitudinal and transversal cracks in the tunnel lining
Longxi highway tunnel	840	22	10	433	The large deformation occured in right haunch of the tunnel, where horizontal convergence was great

The Lanjiayan tunnel is located at one end of the Longmenshan fault, in the core area of the 5.12 Wenchuan Earthquake, Sichuan Province, China, with a length of 8160 m and a buried depth of approximately 1800 m. Results of a geo-stress inversion regression show $\sigma_H > \sigma_h > \sigma_V$ with a maximum principal stress of 72 MPa (Fig. 2). The surrounding rock of the Lanjiayan tunnel is mainly composed of carbonaceous slate, sandstone, and phyllite. This tunnel is classified as a typical high geo-stress soft rock tunnel, which has resulted in long-term

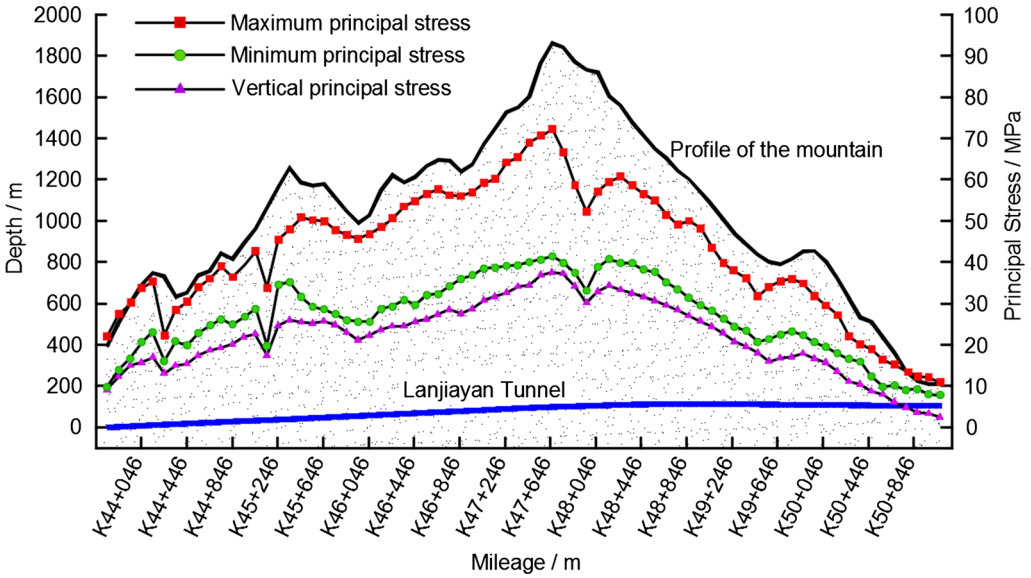

Fig. 2 Geo-stress inversion result of Lanjiayan tunnel

deformations. After excavation of the tunnel, the face usually showed little evidence of water; however, after a while, the groundwater gradually flows down from the fractures and the deformation of the surrounding rock continues to grow due to the high geo-stress. After construction of the secondary lining, the force of the supporting structure still increases because of the intense squeezing pressure, leading to cracking of the primary support and secondary lining, often accompanied by the outflow of groundwater (Fig. 3). Therefore, the development of damage and fracture of deeply buried soft rock at high geo-stress condition could be a gradual evolution process. With the initiation and propagation of fractures, the groundwater gradually penetrates the rock and softens it. Consequently, the self-stabilization capacity of the surrounding rock continues to decrease and the squeezing pressures acting on the supporting structures gradually increase.

In order to investigate the fracture evolution processes in deep-buried soft rocks, uniaxial and conventional triaxial compression tests were conducted under different confining pressures and different water content. The deep-buried carbonaceous slate samples were obtained at a depth of 1020 m from the Lanjiayan tunnel, where the maximum in situ stress was 44.2 MPa. The samples obtained were generally dark gray (Fig. 4a), with a blastopelitic texture and weak-plate structure. Figure 4b shows the carbonaceous slate under polarizing microscope. From X-ray diffraction tests on rock powder (Fig. 4c), it was found that the minerals of carbonaceous slate are mainly illite, chlorite, quartz, and plagioclase in proportions of 40, 33, 40, and 33%, respectively. All the rock samples were taken from the same location in the complete rock mass and were cored and finished into cylinders of 50 mm diameter and 100 mm height.

2.2 Test methods and procedures

In order to study the water-softening damage characteristics of deep-buried carbonaceous slate, the slate specimens

Fig. 3 Failure characteristics of Lanjiayan tunnel

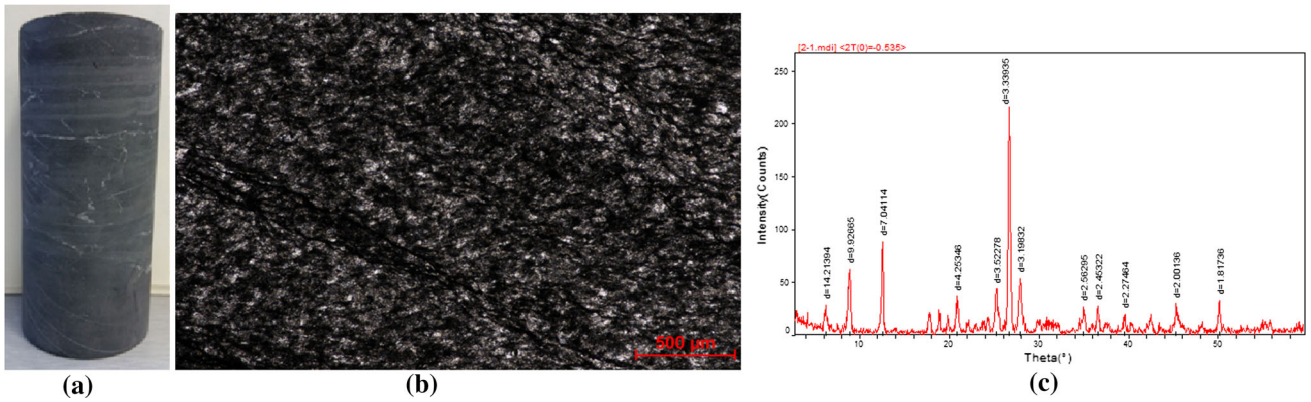

Fig. 4 Photographs of **a** the carbonaceous slate specimen, **b** the polarization microimage; **c** the X-ray diffraction result

were tested under natural and saturated conditions. The natural condition means that the specimens were dried naturally indoors for 5 days after coring and finishing. The average water content of natural carbonaceous slate samples was 1.18%. Figure 5 shows the relationship curve between water content and time the carbonaceous slate specimens were immersed in water. In the first 0–32 h, the water absorption rate of the carbonaceous slate is fast, but in the next 28 h the absorption rate slows down but still steadily increases. After 60 h, absorption significantly decreases. According to the relationship curve, the carbonaceous slate specimen should reach a saturated state after being soaked in water for 72 h; the average water content of saturated carbonaceous slate was measured at 3.16%.

Compression tests were conducted using an MTS815 Flex Test GT rock mechanics experimental system with a PCI-II acoustic emission system (Fig. 6). The maximum loading capacity of the servo-controlled MTS system is 4700 kN, and the maximum confining pressure is 140 MPa. The MTS815 rock mechanics test system can track the whole process of rock failure and obtain the stress–strain curve of rock. The sampling frequency of the AE system is 5 MHz, and the threshold of recording is 40 dB. Uniaxial and conventional triaxial compression tests of carbonaceous slate were performed on both natural and saturated samples (Table 2). The in situ stress of the carbonaceous slate reached 44.2 MPa, which is an extremely high geostress; therefore, the confining pressures used for the conventional triaxial compression tests were set to 15, 30, and 45 MPa.

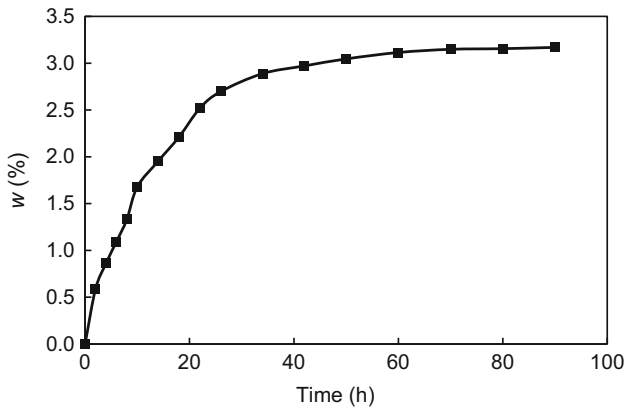

Fig. 5 Relationship curve between water content and soaking time of carbonaceous slate

3 Mechanical properties and fracture evolution

3.1 Uniaxial compression test results

Water is one of the most important factors affecting the stability of underground engineering projects. The complex physical and chemical action between water and rock has a non-negligible influence on the rock's strength, deformation, seepage properties, and failure characteristics. Water has softening, corrosive, and water wedge effects on rock. When water molecules enter into the void spaces of a rock, the cohesion between rock particles is weakened, leading to a reduction in both strength and deformation parameters of the rock. Water is also a solvent that can dissolve some mineral components and cements in rock, while the corrosive effect will produce internal non-uniform stress. At the same time, the decrease in the pore volume can increase pore water pressure and generate additional stress on the deformation and failure processes of rocks, promote the extension of cracks, and eventually decrease the yield and peak strength of rocks. Figure 7 shows the stress–strain curves of carbonaceous slate under natural and saturated states in uniaxial compression tests. In the natural state, the uniaxial compressive strength of carbonaceous slate is 48.41–53.97 MPa. The deep-buried carbonaceous slate is very dense, and there are almost no initial crack compaction or elastic–plastic stages. The failure process of the

Fig. 6 MTS815 Flex Test GT and PCI-II acoustic emission system used to test carbonaceous slate samples

Table 2 Experimental parameters of carbonaceous slates

Sample number	Test type	Moisture state	Water content (%)	Confining pressure (MPa)
D-1	Uniaxial	Natural	1.14	0
D-2	Uniaxial	Natural	1.18	0
D-15	Conventional triaxial	Natural	1.21	15
D-30	Conventional triaxial	Natural	1.18	30
D-45	Conventional triaxial	Natural	1.17	45
B-1	Uniaxial	Saturated	3.14	0
B-2	Uniaxial	Saturated	3.17	0
B-15	Conventional triaxial	Saturated	3.16	15
B-30	Conventional triaxial	Saturated	3.20	30
B-45	Conventional triaxial	Saturated	3.12	45

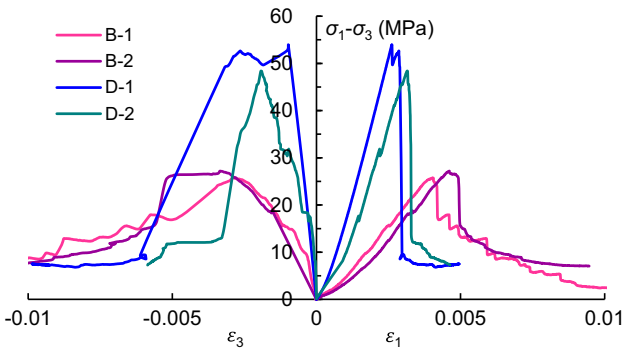

Fig. 7 Stress–strain curves of carbonaceous slate derived from uniaxial compression tests

carbonaceous slate rock shows obvious brittle characteristics as the stress of the slate rapidly decreases at the post-peak stage. However, the mechanical properties and deformation mechanisms in the saturated samples of carbonaceous slate are significantly different; after saturation, there is an initial crack compaction characteristic of the rock at the beginning of loading. The stress at the post-peak stage shows a gradual decrease, indicating that failure of rock is a gradual evolution process. In the natural state, deep-buried carbonaceous slate presents brittle and hard characteristics. But once saturated, the deep-buried carbonaceous slate has features of a soft rock in its strength and deformation characteristics. In the saturated state, the uniaxial compressive strength of carbonaceous slate is 25.73–27.19 MPa, a decrease of 48.3% compared to the natural state. The average elastic moduli of carbonaceous slate in natural and saturated states are 14.84 and 5.83 GPa, respectively, and the average peak strains are 0.288 and 0.432%, respectively. It can be concluded that saturation has a significant effect on the strength and deformation characteristics of deep-buried carbonaceous slate. Therefore, the rock surrounding a deep-buried tunnel under anhydrous condition is relatively more stable. Once groundwater infiltration occurs, the deformation of the surrounding rock increases rapidly, and it is difficult to reach convergence due to the water softening and swelling effect.

Acoustic emissions (AE) are the results of the elastic wave releasing phenomena of initiation, propagation, extension, coalescence of microcracks, and the internal damage of a rock under the action of external loads. Recording AEs from this dynamic evolution process directly presents the growth rate of cracks and the damage development process in rocks. In order to obtain the fracture evolution mechanism of deep-buried carbonaceous slate, the PCI-II acoustic emission system was adopted to monitor the acoustic emission evolution characteristics during the whole deformation process in the rock samples. Figure 8 presents the relationship curves of time with stress and AE counts in uniaxial compression tests. At different water contents, the evolution properties of AE counts are significantly different. The natural state presents as the *main shock* type: The AE activities of carbonaceous slate mainly focus on the failure stage and seldom occur at the pre-peak or post-peak stages. But the saturated samples show *slight shock-main shock-slight shock* characteristics: The saturated carbonaceous slate undergoes quite a few AE activities at the pre-peak and post-peak stages. Moreover, the concentration of AE activities and the AE strength of saturated carbonaceous slate was much lower than in the natural state. The AE evolution law further reflects the brittle failure characteristics of deep-buried carbonaceous slate in the natural state, and its mechanical properties and failure mechanism change into a typical soft rock mode when saturated.

3.2 Triaxial compression test results

Deep-buried underground engineering projects must be able to sustain deformation and failure of the rock at the post-peak stage. At present, the fracture evolution and post-peak strength characteristics of deep-buried rock under high geo-stress conditions are unclear. In order to investigate the influence of high confining pressure and water content on deep-buried carbonaceous slate, conventional triaxial compression tests were conducted on carbonaceous slate in natural and saturated states at confining pressures of 15, 30 and 45 MPa.

The stress–strain curves are presented in Fig. 9. Similar to the uniaxial compression tests, the carbonaceous slate shows brittle failure characteristics in the natural state; the nonlinear deformation feature is not obvious at the pre-peak stage and the stress deceases significantly at the post-peak stage. The peak strength and elastic modulus of carbonaceous slate increase with the increase in the confining pressure. At confining pressures of 15, 30 and 45 MPa, the peak strengths were 132.2, 224.6 and 299.1 MPa, respectively, and the elastic moduli were 41.1, 68.9, and 79.6 GPa, respectively. Compared with the natural state, saturated samples of carbonaceous slate showed obvious ductility and plastic deformation properties. At confining pressures of 15, 30, and 45 MPa, the peak strengths were 96.7, 178.9, and 239.9 MPa, respectively, with elastic moduli of 25.6, 45.7, and 54.6 GPa, respectively. At present, the Coulomb strength criterion ($\sigma_1 = M\sigma_3 + N$) is widely used in rock mechanics to describe the strength characteristics of rock, in which M and N are the strength parameters related to the cohesion and internal friction angle of rock. Figure 10 presents the relationship curves of the confining pressure with peak strength and elastic modulus of carbonaceous slate at different water contents. It can be seen that the Coulomb strength criterion well reflects the compressive strength under different water contents. The cohesion of deep-buried carbonaceous slate decreases from 4.6 to 2.8 MPa after water infiltration, with a decrease in the angle of internal friction from 23.6° to 21.2°. Therefore, the softening effect seen from an increase in water content mainly reduces the cohesion of the slate. As the confining pressure increases, the softening coefficient gradually increases (Table 3). Just because of the compaction effect of high confining pressure, the surrounding rock was usually without water immediately after excavation of the Langjiayan tunnel. However, the groundwater would gradually flow down with the evolution

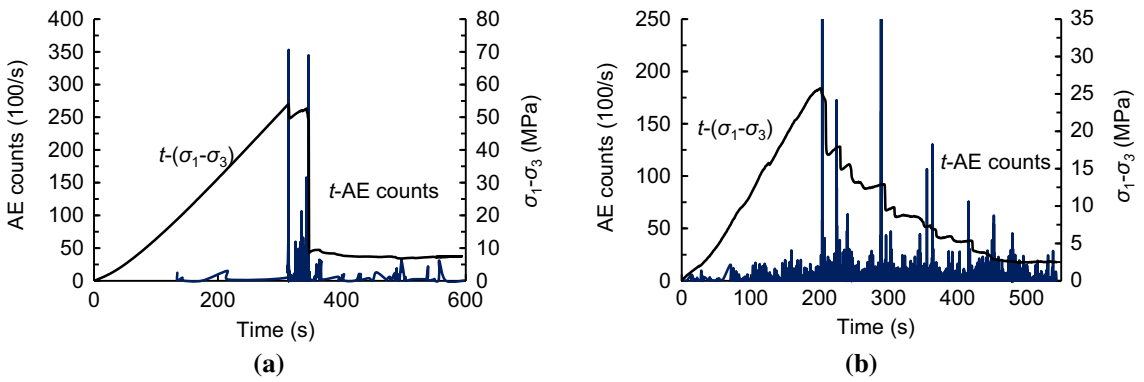

Fig. 8 Relationship curves of time with stress and AE counts in uniaxial compression tests. **a** D-1, **b** B-1

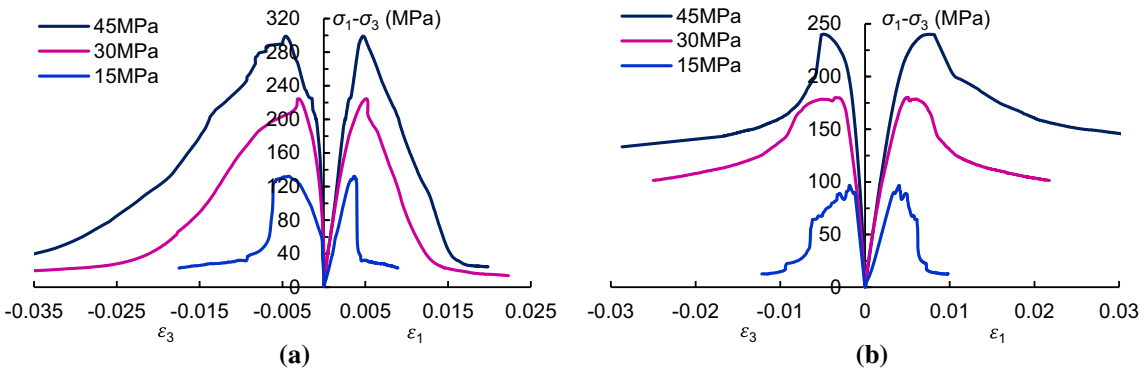

Fig. 9 Stress–strain curves of carbonaceous slate in triaxial compression tests. **a** Natural, **b** saturated

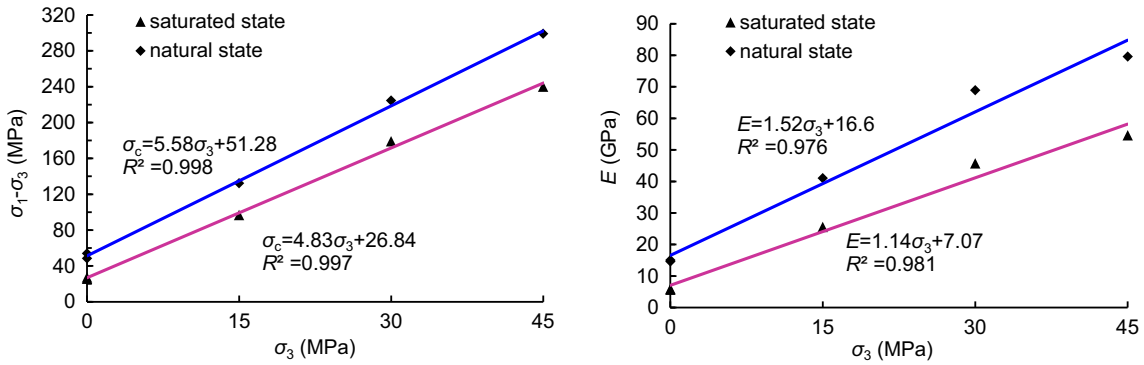

Fig. 10 Relationship curves of confining pressure with peak strength and elastic modulus of carbonaceous slate

Table 3 Mechanical properties of carbonaceous slates

Sample number	Peak strength/MPa	*E*/GPa	Peak strain/%	Softening coefficient (%)
D-uniaxial	51.2	14.8	0.29	–
D-15	133.2	41.1	0.36	–
D-30	224.6	68.9	0.50	–
D-45	299.1	79.6	0.48	–
B-uniaxial	26.4	5.8	0.42	51.7
B-15	96.7	25.6	0.41	73.1
B-30	178.9	45.7	0.51	79.7
B-45	239.9	54.6	0.76	80.2

of fracture in carbonaceous slate due to the tunneling activities.

It should also be noted that the peak strain of slate in the saturated state was larger than in the natural state, which means that the saturated slate has greater ductility. Based on the mechanical characteristics observed at the post-peak stage, the natural slate can be considered as a brittle rock; the stress drops quickly, and there is hardly any residual strength after rock failure. When saturated, the plasticity feature of carbonaceous slate is enhanced; the residual strength is significantly larger than in the natural state and it increases with tan increase in the confining pressure.

Relationship curves of time with stress and AE counts in triaxial compression tests are shown in Fig. 11. When confining pressure is 15 MPa, the AE activities of deep-buried carbonaceous slate act mainly as seen in the failure stage and seldom appear at the pre-peak and post-peak stages (Fig. 11a). When the confining pressure increases to 30 MPa, the AE activities of carbonaceous slate become more active at the post-peak stage (Fig. 11c). When confining pressure is 45 MPa, the concentration of AE activity

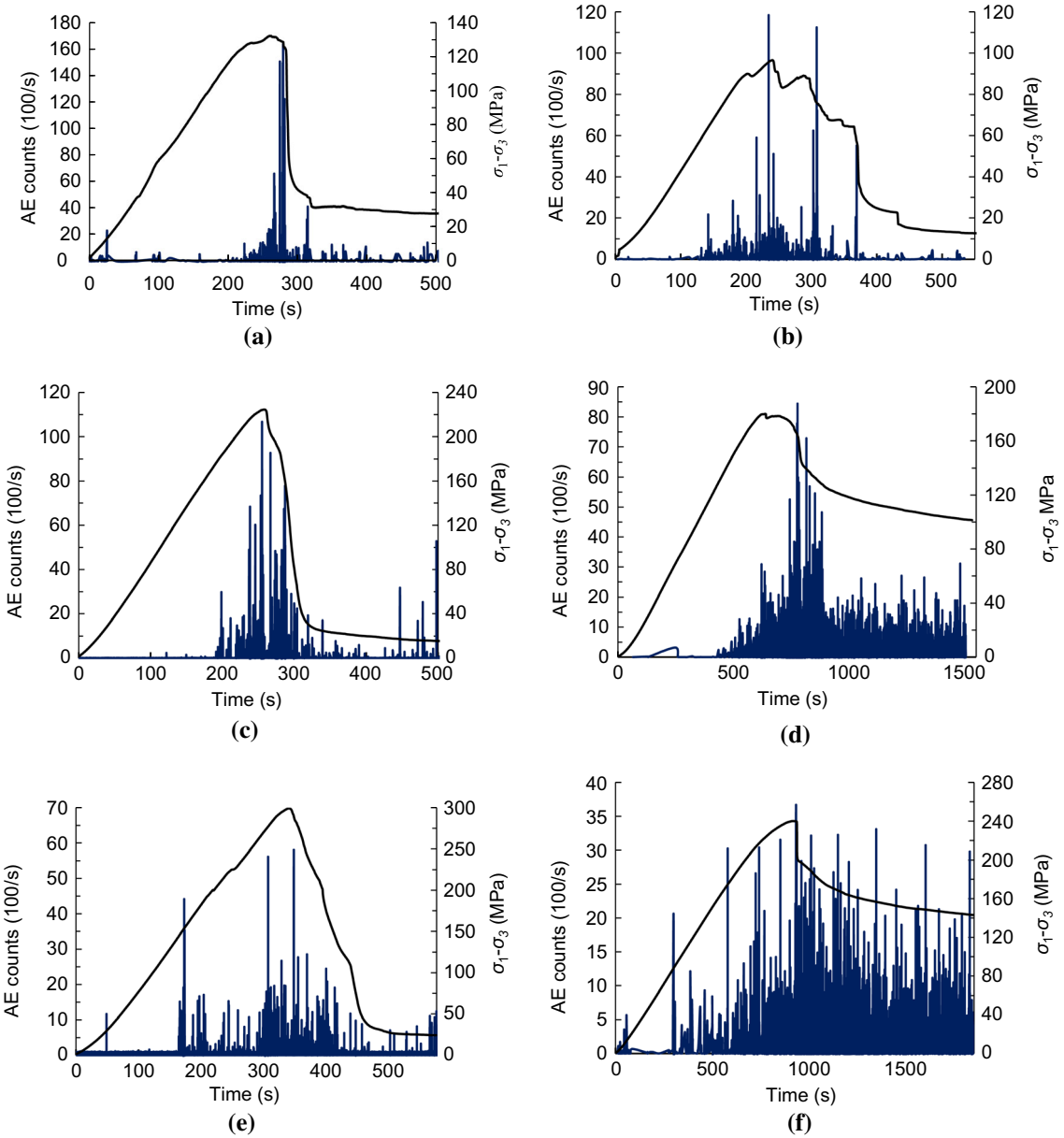

Fig. 11 Relationship curves of time with stress and AE counts in triaxial compression tests. **a** D-15, **b** B-15, **c** D-30, **d** B-30, **e** D-45, **f** B-45

and the strength of carbonaceous slate is further reduced (Fig. 11e), indicating that the pre-peak damage to the slate is small and failure occurs more suddenly under low confining pressure. However, as the confining pressure increases, the failure of carbonaceous slate becomes a gradual evolution process, and the plasticity is enhanced; many secondary fractures will be generated and extended after the failure of the rock. In the natural state, the AE activities recorded in the carbonaceous slate samples were more concentrated than in the saturated state with the maximum instantaneous AE counts at confining pressures of 15, 30 and 45 MPa of 16,389, 10,664 and 5695, respectively. In the saturated state, the AE activities of carbonaceous slate appeared early and were more pronounced in the post-peak stage; the maximum instantaneous AE counts at confining pressures of 15, 30 and 45 MPa were 11,847, 8443, and 3557, respectively. The maximum instantaneous AE counts for the saturated carbonaceous slate were observed to be smaller than those in the natural state, and they gradually decreased with an increase in the confining pressure. Thus, the fragmentation behavior at the post-peak stage for carbonaceous slate under high confining pressure could be more significantly than under low confining pressure.

4 Energy mechanism

4.1 Uniaxial compression test results

It is understood that damage evolution and final unstable failure of materials are driven by energy. Based on the energy evolution mechanism, the deformation and failure of materials are accompanied by energy input, energy accumulation, energy dissipation, and energy release. Thus, microseismic monitoring system is now widely employed to record actual crack events during tunnel excavation. Cracking is accompanied by the release of strain energy in the form of releasing elastic waves that affect the surrounding rock mass (Fig. 12). Similar to the microseismic monitoring system, an acoustic emission system could be used to detect the fracture evolution process and internal damage to the rock samples in a laboratory setting. AE systems measure the transient of elastic waves that are generated during the deformation and failure processes in rock and can reflect the closure of existing microcracks, crack initiation and propagation, rock failure, and the fragmentation at the post-peak stage.

The strain energy of a rock can be divided into three kinds, where U denotes the total energy absorbed by the rock, U_e represents elastic strain energy, and U_d represents dissipated energy. The computational expression for U and U_e are given as follows [31, 33]:

$$U = U_e + U_d \tag{1}$$

$$U = \int \sigma_1 d\varepsilon_1 + 2\int \sigma_3 d\varepsilon_3 \tag{2}$$

$$U_e = \frac{1}{2E_0}\left[\sigma_1^2 + 2\sigma_3^2 - 2v(\sigma_3^2 + 2\sigma_1\sigma_3)\right]. \tag{3}$$

Figure 13 shows the typical strain energy evolution curves and AE energy evolution curves of carbonaceous slate under uniaxial compression. During the deformation and failure processes of deep-buried carbonaceous slate, the strain energy evolution curves match well with the AE energy evolution curves. The energy evolution characteristics of carbonaceous slate in the natural state represent a *main shock*-type event, and this changes to the *slight shock–main shock–slight shock* type after saturation. In the natural state, the concentration of AE energy and the strength of carbonaceous slate are higher than in the saturated state, which means that the rock's brittle failure characteristics are weakened after saturation.

At the pre-peak stage, the total energy and elastic strain energy curves show upward-concave and nonlinear evolution features; the energy absorbed by the rock is mainly stored in the form of elastic strain energy. This means that the energy behavior is mainly expressed as energy accumulation and energy hardening at this stage. When the carbonaceous slate is in its natural state, there are almost no AE energy releases in the pre-peak stage, while there are some small-magnitude AE activities when saturated.

When natural slate reaches its peak strength, the elastic strain energy is released instantly during the stress drop process. On the other hand, according to the AE energy evolution law, the elastic strain energy gradually decreases and the dissipated energy gradually increases after rock failure. However, when the slate is saturated, the energy storage limit is 40.8 kJ/m^3, which is lower than the 60.4 kJ/m^3 limit of natural slate. During the post-peak stage, energy absorbed by the rock is converted to dissipation

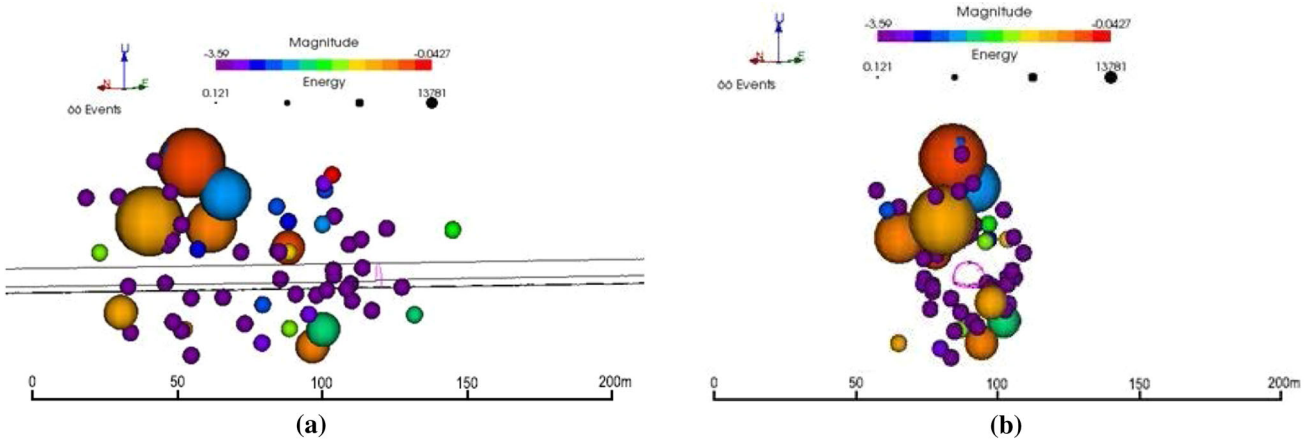

Fig. 12 Results of microseismic monitoring in a tunnel excavation. **a** Longitudinal perspective of tunnel, **b** transverse perspective of tunnel

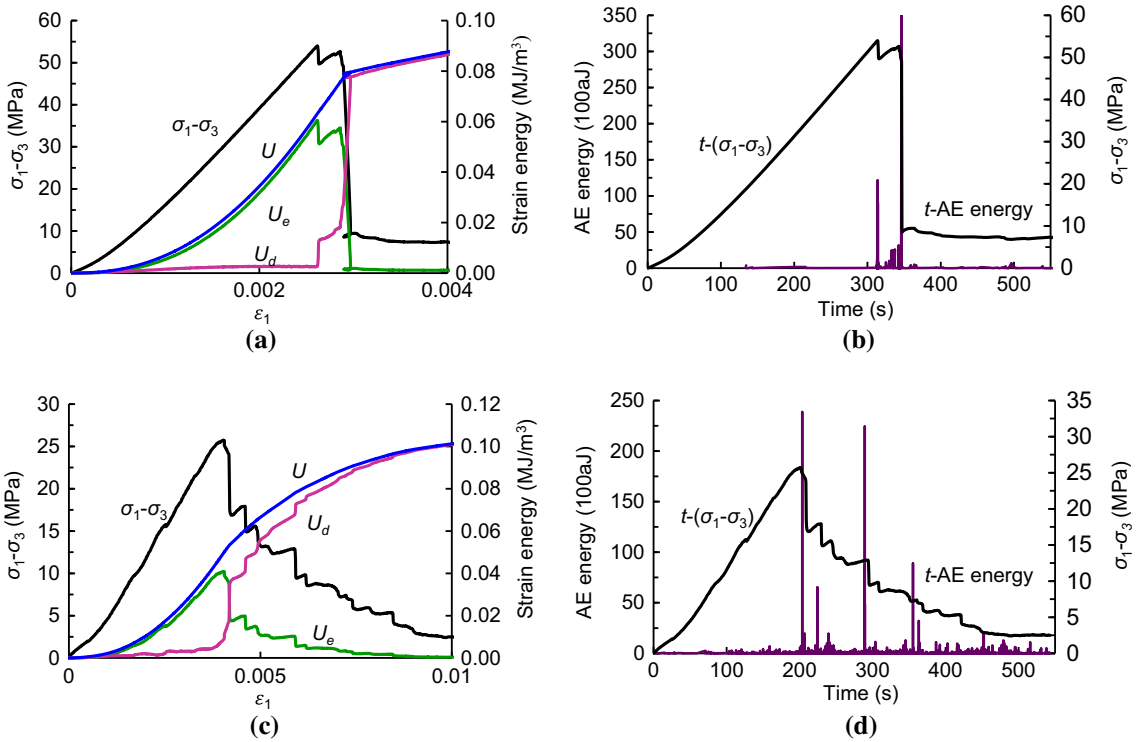

Fig. 13 Energy evolution curves and AE energy evolution curves in uniaxial compression tests. **a** Strain energy of D-1, **b** AE energy of D-1, **c** strain energy of B-1, **d** AE energy of B-1

energy. The dissipated energy supports the extension of interior cracks and shear rupture along slip planes. The natural carbonaceous slate shows very little energy release in this stage, while the saturated samples show continuous fracture and energy evolution. This means that the carbonaceous slate in a natural state is better able to store and release energy, while the fracture and energy evolution characteristics of saturated slate are more obvious.

4.2 Triaxial compression test results

Figure 14 shows the strain energy evolution curves of carbonaceous slate under different confining pressures and water content. During the initial compressive deformation stage and the linear-elastic deformation stage, the energy behavior mainly presents as energy accumulation and energy hardening. At these two stages, the total energy curve and elastic strain energy curve are basically parallel. After reaching the cracking strength, the rock enters the nonlinear deformation stage. The total energy curve begins to diverge from the elastic strain energy curve. As the internal cracks steadily extend, dissipated energy increases faster and faster. When the stress is close to the peak strength, the elastic strain energy gradually attains its storage limit. Once the slate reaches its peak strength, the elastic strain energy is released and the dissipated energy increases rapidly due to macroscopic damage. It can be seen that the carbonaceous slate is better able to release energy under low confining pressure and in its natural state. When saturated and at high confining pressure, the evolution curve of dissipated energy is smoother. In the saturated state, the carbonaceous slate has more residual elastic strain energy and tends to present shear failure characteristics. Natural slate undergoes more tensile fractures, which leads to lower residual strength and less residual elastic strain energy.

At the confining pressures of 15, 30 and 45 MPa, the energy storage limits of carbonaceous slate in the natural state are 198.7, 396.9 and 671.6 kJ/m^3, respectively, while in the saturated state they are 169.1, 328.7 and 586.9 kJ/m^3, respectively (Table 4). The energy storage and rapid energy release capability of the slate decreases with an increase in water content, and, because of this, a rock burst often occurs during excavation of a deep-buried tunnel in a non-water hard rock mass. In the saturated state, at the peak strength point, the proportion of elastic strain energy (U_e/U) is smaller than in the natural state, and the proportion of dissipated energy (U_d/U) is larger (Table 4). In addition, the U_e/U at the peak strength point decreases with an increase in confining pressure. Therefore, compared to saturated slate and high confining pressure, the interior fractures and damage to deep-buried natural carbonaceous slate and low confining pressure at the pre-peak stage are relative small.

Aubertin et al. [1] defined the ratio of dissipated energy and elastic strain energy of rocks at the peak strength point

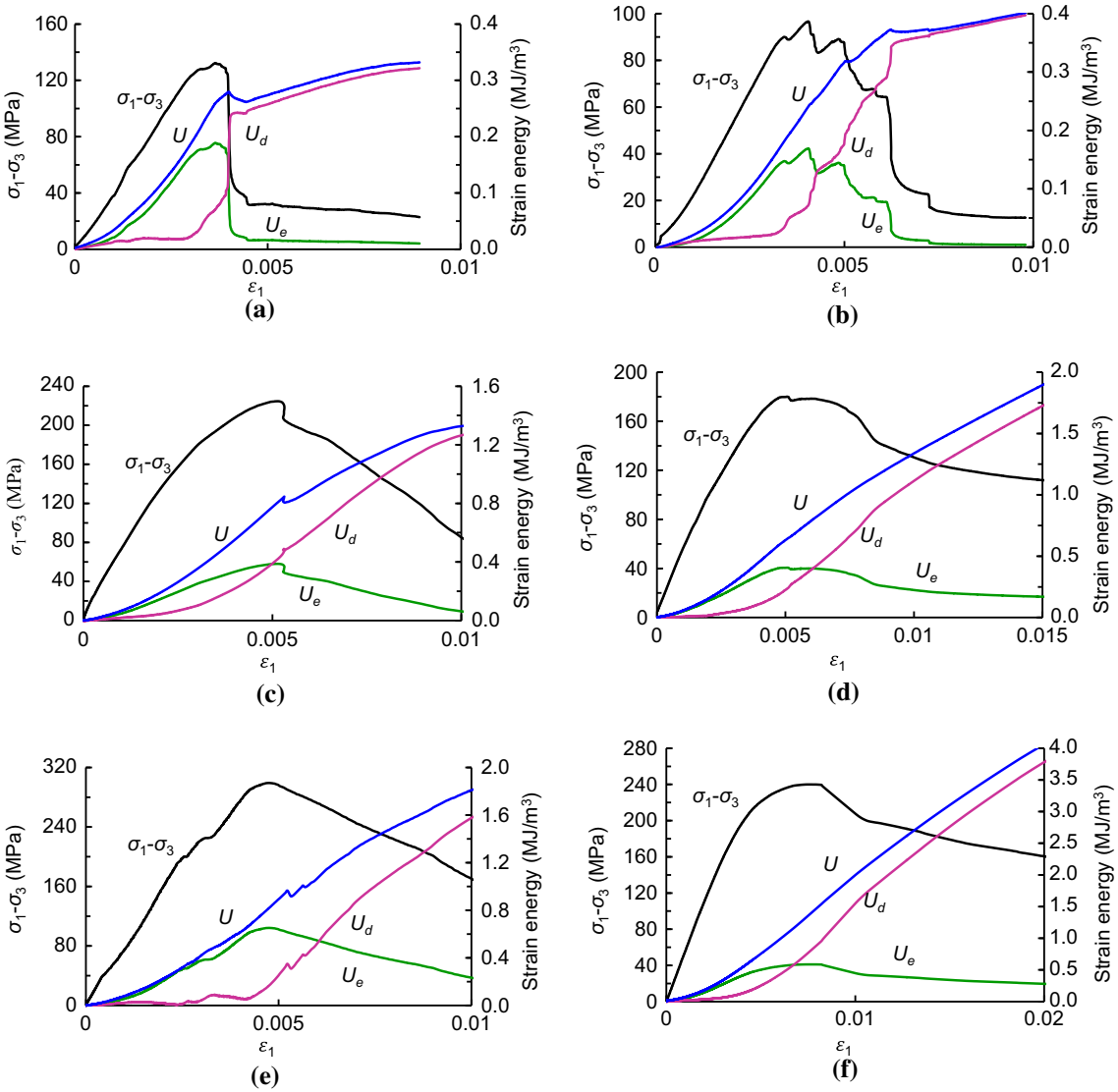

Fig. 14 Strain energy evolution curves of carbonaceous slate in triaxial compression tests. **a** D-15, **b** B-15, **c** D-30, **d** B-30, **e** D-45, **f** B-45

Table 4 Energy properties of carbonaceous slates

Specimen	U_e^{max} (kJ/m^3)	Strength peak point		*BIM*	Maximum AE energy (100 aJ)	AE evolution type
		U_e/U	U_d/U			
D-1	60.4	0.954	0.046	0.048	348.0	Main shock
D-2	57.6	0.908	0.092	0.101	369.5	Main shock
D-15	198.7	0.812	0.188	0.232	255.9	Main shock–slight shock
D-30	396.9	0.727	0.273	0.375	96.6	Main shock–slight shock
D-45	671.6	0.615	0.385	0.626	47.5	Foreshock–main shock–slight shock
B-1	40.8	0.886	0.114	0.129	238.7	Slight shock–main shock–slight shock
B-2	44.6	0.855	0.145	0.169	269.5	Main shock–slight shock
B-15	169.1	0.701	0.299	0.426	149.3	Slight shock–main shock–slight shock
B-30	328.7	0.665	0.335	0.504	67.4	Slight shock–main shock–after shock
B-45	586.9	0.419	0.581	1.38	31.1	Foreshock–main shock–after shock

(U_e/U_d) as the Brittleness Modifying Coefficient (*BIM*). The larger the *BIM* is, the stronger is the ductility of rock. It is found that the *BIM* of carbonaceous slate increases as the confining pressure increases, while the *BIM* of saturated carbonaceous slate is larger than in the natural state. This further validates the conclusions obtained from the acoustic emissions and energy evolution law.

Figure 15 shows the AE energy evolution curves of carbonaceous slate during triaxial compression tests. The curves reveal the energy release characteristics and damage evolution mechanism of the rock. At a confining pressure of 15 MPa, the AE energy evolution characteristics of the slate in the natural and saturated states present the *main shock–slight shock*-type event and *slight shock–main shock-slight shock*-type event, respectively, and as the confining pressure increases to 30 MPa they reveal *main shock–slight shock*-type and *slight shock–main shock–after shock*-type events. At a confining pressure of 45 MPa, the AE evolution for the natural and saturated samples changes to *foreshock–main shock–slight shock-* and *foreshock–main shock–after shock*-type events, respectively. However, once the rock is saturated, the concentration of AE energy and energy strength decrease. These results have lead to the use of water injection into the surrounding rock to prevent rock bursts during the excavation of deep-buried underground engineering facilities. In the natural state, the maximum AE energy values of carbonaceous slate at confining pressures of 15, 30, and 45 MPa are

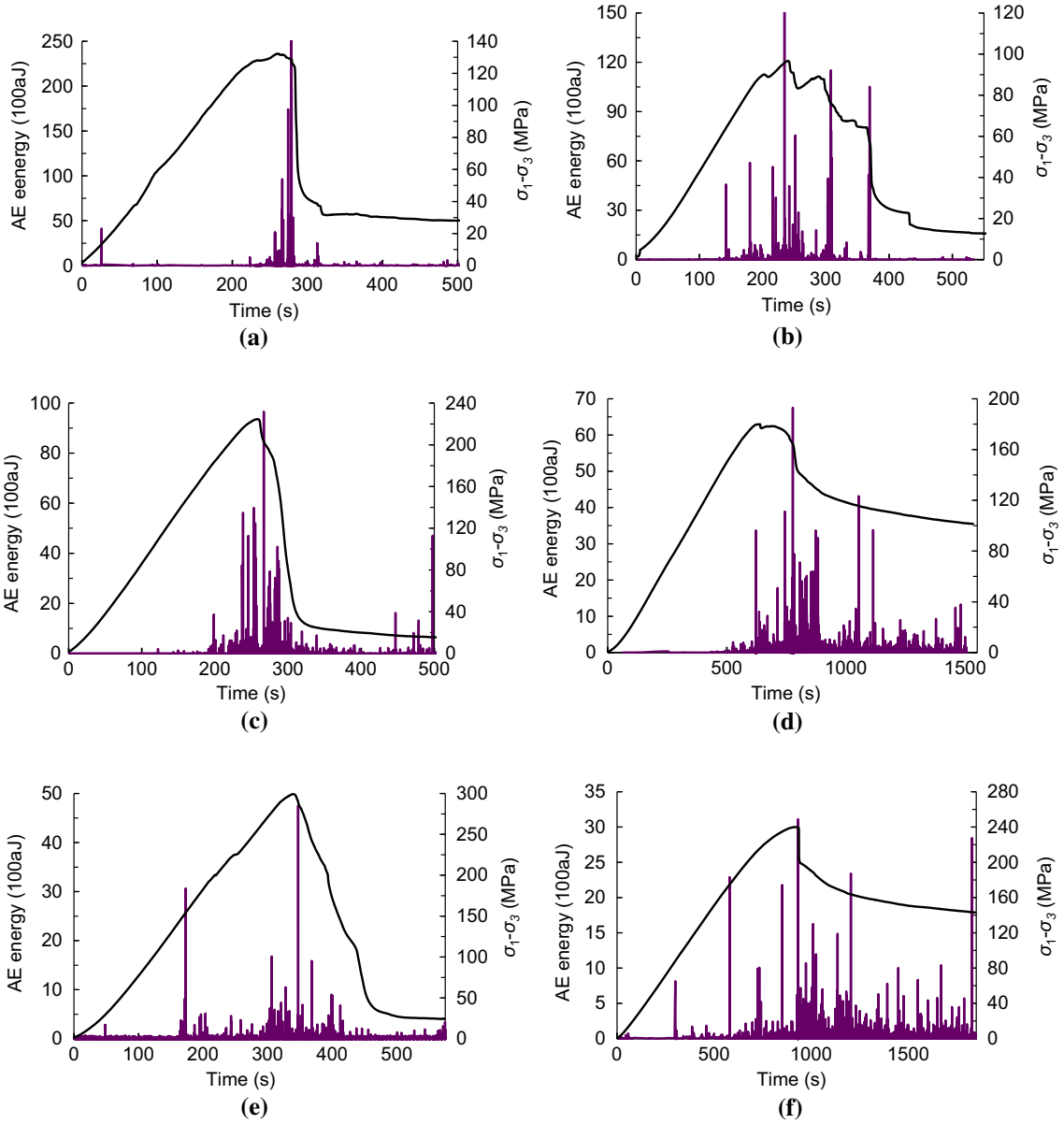

Fig. 15 Relationship curves of time with stress and AE energy in triaxial compression tests. **a** D-15, **b** B-15, **c** D-30, **d** B-30, **e** D-45, **f** B-45

255.9×10^2, 96.6×10^2, and 47.5×10^2 aJ, respectively; in the saturated state, and they decrease to 149.3×10^2, 67.4×10^2 and 31.1×10^2 aJ, respectively. As the confining pressure increases, the concentration AE energy and maximum AE energy gradually decreases. Based on the AE energy evolution law, carbonaceous slate exhibits brittle failure under low confining pressure when in its natural state. However, when confining pressure and water content increases, ductile and plastic characteristics of carbonaceous slate are improved; its crack evolution and energy release are progressive failure processes.

5 Damage evolution mechanism

5.1 Discussion of damage stress thresholds based on energy mechanisms

The transformation of energy is driven by energy-hardening and energy-softening mechanisms. The energy-hardening mechanism transforms external energy into elastic strain energy and stores it inside the rock. The energy-softening mechanism transforms elastic strain energy into heat and other forms of energy. The energy mechanism reflects the damage evolution process and also plays an important role in studying the mechanical properties and the failure mechanism of rock.

During the deformation and failure processes in carbonaceous slate, the elastic stain energy proportion (P_e) is the ratio of elastic strain energy and total energy of the rock, and the dissipated energy proportion (P_d) is the ratio of dissipated energy and total energy of rock. Based on the elastic strain energy proportion and dissipated energy proportion curves of carbonaceous slate shown in Fig. 16 (saturated samples and 45 MPa confining pressure), it can be seen that the energy curves show strong regularity during the whole deformation and failure processes in carbonaceous slate. The elastic strain energy proportion curve declines first and then rises, followed by a gradual decline until it finally maintains a certain residual value. In contrast, the dissipated energy proportion curve rises first and then declines after which it gradually rises and finally remains stable.

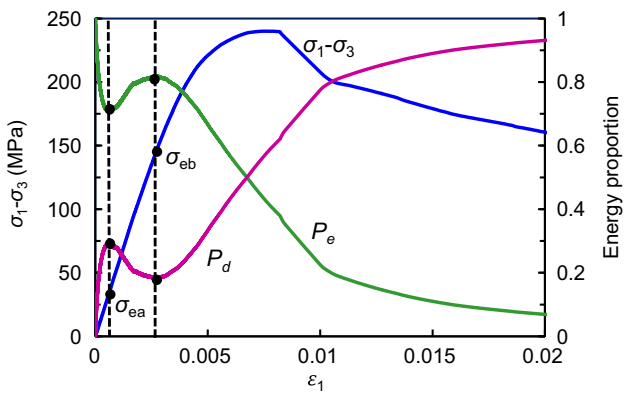

Fig. 16 Evolution curves of P_e and P_d of B-45

In view of the S-shaped evolution law of energy proportion, two damage stress thresholds, σ_{ea} and σ_{eb}, can be obtained. During the early loading stage, the dissipated energy proportion increases gradually. This is because the closure of initial cracks and friction of rock particles can dissipate some energy. However, the elastic strain energy proportion is larger than the dissipated energy proportion at this stage. When the rock reaches the stress threshold σ_{ea}, the elastic strain energy proportion gradually increases and the dissipated energy proportion gradually decreases. The energy accumulation mechanism of the rock is strengthened. Accordingly, the stress threshold σ_{ea} can be regarded as an indication that the rock is entering the energy-hardening stage. After the rock reaches the stress threshold σ_{eb}, the elastic strain energy proportion gradually decreases, and the dissipated energy proportion starts to steadily increase. This indicates that the interior cracks and damage in the rock are increasing. Therefore, the stress threshold σ_{eb} can be regarded as the mark of the rock entering the energy-softening stage.

Based on the strength feature and the crack volumetric strain, Martin and Chandler [17, 18] proposed the terms closure stress σ_{cc} and crack initiation stress σ_{ci}. Closure stress σ_{cc} is the stress of the rock as it changes from the initial compaction stage to the elastic deformation stage. Crack initiation stress σ_{ci} indicates the beginning of the stable growth of microcracks. Table 5 shows the experimental results of σ_{ea}, σ_{cc}, σ_{ci}, and σ_{eb} of deep-buried carbonaceous slate. The damage stress threshold σ_{ea} is smaller than the closure stress σ_{cc}, which means that the energy accumulation in slate is strengthened before the slate enter the elastic deformation stage. When the damage stress threshold σ_{eb} is larger than the crack initiation stress σ_{ci}, it indicates that the energy mechanism in slate is still in the energy-hardening condition at the early inner crack extension stage. When the slate enters the energy-softening stage, the energy dissipation and energy release of the rock gradually increase with damage growth. Based on the energy evolution mechanism, the damage stress thresholds of σ_{ea} and σ_{eb} are important to further understand the damage evolution process and fracture evolution mechanism of rock.

Table 5 shows that the ratio of closure stress and peak strength (σ_{cc}/σ_c) of deep-buried carbonaceous slate is between 0.21 and 0.32, and the ratio of crack initiation stress and peak strength (σ_{ci}/σ_c) is between 0.45 and 0.55. Compared with the σ_{cc}/σ_c and σ_{ci}/σ_c of slate which have little change at different confining pressures and different

Table 5 Thresholds of carbonaceous slates in tests

Specimen	σ_{ea}/MPa	σ_{ea}/σ_c	σ_{cc}/MPa	σ_{cc}/σ_c	σ_{ci}/MPa	σ_{ci}/σ_c	σ_{eb}/MPa	σ_{eb}/σ_c
D-2	4.4	0.09	12.5	0.26	24.7	0.51	46.5	0.96
D-15	17.1	0.13	42.7	0.32	62.4	0.47	117.6	0.89
D-30	49.8	0.22	73.9	0.32	104.8	0.46	156.6	0.69
D-45	59.8	0.19	90.1	0.30	141.2	0.47	191.9	0.64
B-1	2.3	0.09	4.6	0.18	14.4	0.56	24.2	0.94
B-2	2.7	0.10	5.1	0.19	14.9	0.55	25.3	0.93
B-15	10.1	0.11	22.4	0.23	51.7	0.53	84.3	0.87
B-30	28.5	0.15	46.1	0.25	89.6	0.50	111.8	0.63
B-45	35.5	0.15	55.5	0.23	109.9	0.45	150.9	0.62

water contents, the σ_{ea}/σ_c and σ_{eb}/σ_c are more sensitive with confining pressure and water content. The σ_{ea}/σ_c is between 0.08 and 0.22, and it increases with the increases in confining pressure. It is suggested that the slate enters the energy accumulation and energy-hardening stage earlier at low confining pressure. Besides, the σ_{eb}/σ_c is between 0.62 and 0.96. In the uniaxial compression tests, the σ_{eb}/σ_c is up to 0.96, and it is close to the peak strength, which means that the brittle failure would occur in a short period of time and small stress increment. At the confining pressures of 15, 30, and 45 Mpa, the σ_{eb}/σ_c of carbonaceous slate in the natural state are 0.89, 0.69, and 0.64, respectively. While in the saturated state, the σ_{eb}/σ_c are 0.87, 0.63, and 0.62, respectively. The σ_{eb}/σ_c of carbonaceous slate is decreased with the increase in water content and confining pressure. This further certifies that the plasticity and ductility of rock mass are enhanced under the condition of rich water and high geo-stress, and the deep-buried carbonaceous slate could enter the energy dissipation and energy-softening stage earlier. On account of this, the AE energy evolution type of carbonaceous slate presents the *main shock* type under low confining pressure and presents the *foreshock–main shock* type under high confining pressure. And this could also reveal the reason why the carbonaceous slate in saturated state has much more acoustic emission events at the pre-peak stage than in natural state.

5.2 Damage evolution process of carbonaceous slate

During deformation, carbonaceous slate undergoes damage evolution and gradual degradation processes. In order to study the damage evolution process of rock, some macroscopic characteristic variables such as elastic modulus, yield stress, and velocity of ultrasonic waves are often used to classify the degree of damage in the rock,. For practical engineering projects in rock masses, the accumulated elastic strain energy is the main energy source for cracks and failure. In situations where there is a high geo-stress background, the sudden energy release caused by an excavation could promote the failure of the rock and lead to dynamic disasters, such as rock bursts. The damage evolution curve of B-45 is presented in Fig. 17. According to the S-shaped evolution law, the damage evolution process of deep-buried carbonaceous slate can be divided into four stages.

- Stage 1: the initiation of damage. From the initial loading to the σ_{eb}, the dissipated energy proportion first increases and then decreases. During this stage, the damage to the carbonaceous slate is small, and dissipated energy and AE activities are quite few.
- Stage 2: the stable development of damage. When carbonaceous slate reaches the damage stress threshold σ_{eb}, the dissipated energy and accumulated AE energy begin to increase gradually; cracks and damage are steadily generated.
- Stage 3: the damage acceleration and failure phase. When carbonaceous slate enters this stage, inner damage to the rock fabric increases rapidly. At this stage, the dissipated energy increases quickly; AE counts and AE energy rate reach their maximum values.
- Stage 4: the residual damage phase. Carbonaceous slate enters the residual damage stage after macroscopic failure. The energy absorbed by the rock at this stage is converted into dissipated energy. Dissipated energy and accumulated AE energy still increase steadily, but the energy increment and the AE events are related to the confining pressure and water content.

The damage coefficient D (range from 0 to 1) is generally used to define the extent of rock damage; $D = 0$ indicates no damage and $D = 1$ means that the rock has failed completely. However, the carbonaceous slate still has the ability to absorb energy and retain some residual energy after it reaches its peak strength. In view of this, the

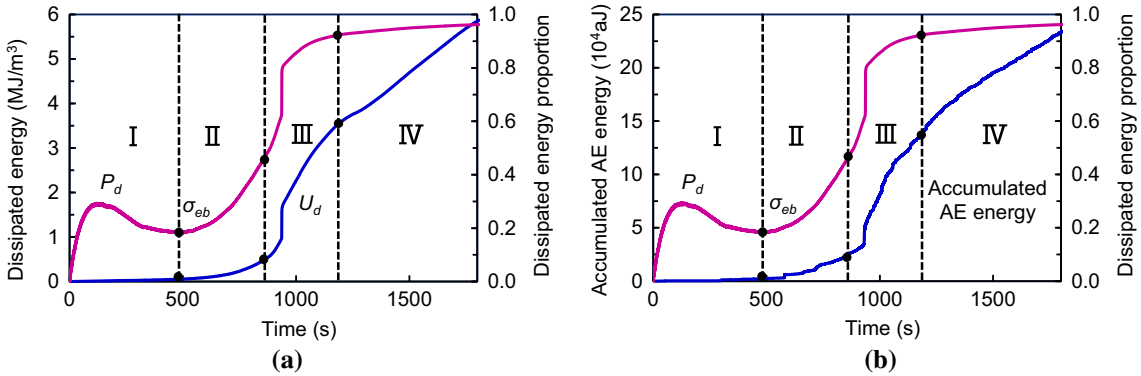

Fig. 17 Damage evolution curves based on dissipated energy and accumulated AE energy of B-45

energy evolution characteristics and damage evolution mechanism of slate can be systematically analyzed at the pre-peak stage. In this paper, the damage coefficient D of slate at the peak strength point is defined as 1. Therefore, normalized damage variables D_{de} and D_{AE}, which are related to the dissipated energy and the accumulated AE energy, can be calculated using the following equations:

$$D_{de} = \frac{U_d}{U_p} \tag{4}$$

$$D_{AE} = \frac{C_{AE}}{C_P} \tag{5}$$

where U_d is the dissipated energy, U_p is the dissipated energy at peak strength, C_{AE} is the accumulated AE energy, C_P is the accumulated AE energy at peak strength.

Damage coefficient evolution curves based on the energy mechanism observed in sample B-45 are shown in Fig. 18. The two damage coefficient D_{de} and D_{AE} are in good agreement, both of them reflecting the degree of damage to carbonaceous slate during the deformation process. Table 6 lists the damage coefficient of carbonaceous slate at the damage stress thresholds σ_{ea} and σ_{eb}. The degree of damage to the carbonaceous slate at the σ_{ea} and σ_{eb} decreases with the confining pressure and water content, which means that the rock enters the energy-hardening stage and energy-softening stage earlier at high confining pressures or saturated state corresponding to the AE characteristics. Using D-1 as an example, the σ_{eb}/σ_c and D_{de} are 0.95 and 19.5%, which means that sample D-1 has to complete 80.5% of its damage in only a $0.05\sigma_c$ stress increment. Sample B-45 will complete 92.9% of its damage in a 0.38 σ_c stress increment. Therefore, the combination of the two parameters can reflect the different damage and failure mechanisms of carbonaceous slate under different conditions.

Table 6 Damage coefficient of specimens at damage stress thresholds, σ_{ea} and σ_{eb}

Specimen	σ_{ea}			σ_{eb}		
	σ_{ea}/σ_c	D_{de}/%	D_{AE}/%	σ_{eb}/σ_c	D_{de}/%	D_{AE}/%
D-1	0.08	5.4	5.6	0.95	19.5	18.6
D-2	0.09	5.1	4.7	0.96	18.6	17.9
D-15	0.13	2.8	2.6	0.89	12.6	11.8
D-30	0.22	1.5	0.6	0.69	9.1	8.6
D-45	0.19	1.6	0.7	0.64	5.6	5.9
B-1	0.09	5.8	4.9	0.94	24.3	22.9
B-2	0.10	5.3	4.4	0.93	23.8	21.8
B-15	0.11	3.0	2.8	0.87	15.6	16.5
B-30	0.15	1.8	1.3	0.63	11.8	9.6
B-45	0.15	1.6	0.9	0.62	7.1	7.7

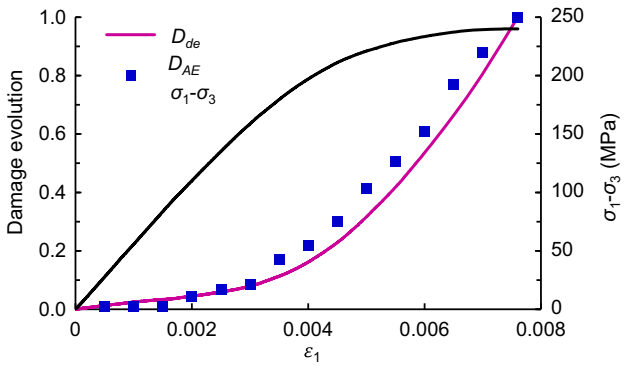

Fig. 18 Damage coefficient evolution curves based on energy mechanism observed in B-45

Brittleness is an important index for evaluating the mechanical properties of rock [16, 39]. The term brittle rock indicates that there is no obvious deformation prior to the rock failure; the rock has high compressive strength and small tensile strength. A brittle rock often has good energy storage capacity but this energy can be rapidly released as the rock fails. Accordingly, a new brittleness energy index is proposed based on the damage evolution mechanism and the energy storage capacity of rock:

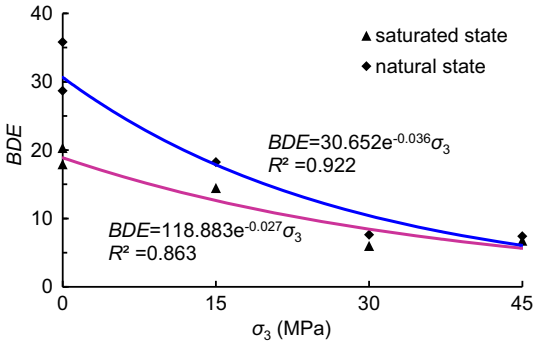

Fig. 19 Relationship curves between *BED* and confining pressure of carbonaceous slate

$$BDE = (1 - D_{de})\frac{\sigma_c}{\sigma_c - \sigma_{eb}}\log_{10}U_e^{max}, \quad (6)$$

where D_{de} is the damage degree at the σ_{eb}, σ_c is the peak strength, U_e^{max} is the energy storage limit.

Brittleness energy indexes of carbonaceous slate are shown in Fig. 19. In both the natural and saturated states, the brittleness energy index *BDE* of carbonaceous slate gradually decrease as the confining pressure increases. Consistent with the strength law, the brittleness energy index of slate in a saturated state is less sensitive to changes in confining pressure. It is interesting that the *BDE* shows little change from a confining pressure of 30 MPa to the extremely high confining pressure of 45 Mpa. This illustrates that the energy storage limit plays a major role in the brittleness energy index under high confining pressure. In the natural state, the *BDE* is larger than in the saturated stat; when saturated, the influence of confining pressure on the *BDE* is lower than in natural slate. Therefore, the brittleness energy index *BDE*, which considers complete 1 to D_{de} damage in the $\sigma_c - \sigma_{eb}$ stress increment and takes the energy storage limit into account, can evaluate the damage evolution mechanism and the brittleness of deep-buried carbonaceous slate with the change of confining pressure and water content.

6 Conclusion

1. High confining pressure and water content greatly influence the mechanical properties and fracture evolution mechanism of deep-buried carbonaceous slate. The mechanical characteristics of slate increase with increases in the confining pressure, and the softening effect of water mainly reduces the cohesion of carbonaceous slate, but decreases with an increase in the confining pressure.
2. With an increase in the confining pressure and water content, the acoustic emission events and dissipated energy gradually increase at the pre-peak and post-peak stages. Thus, the AE evolution type in the natural state and at low confining pressure usually presents as *main shock*-type events, changing to *foreshock–main shock–after shock*-type events when saturated and at high confining pressure. As the confining pressure and water content increase, the ductility and plasticity fracture mechanisms of deep-buried carbonaceous slate are enhanced.
3. Based on the S-shaped energy evolution law, the damage stress thresholds σ_{ea} and σ_{eb} are obtained. The σ_{ea} and σ_{eb} can be considered to be the indicators of the rock entering the energy-hardening and energy-softening stages. Compared with the σ_{cc}/σ_c and σ_{ci}/σ_c, the σ_{ea}/σ_c and σ_{eb}/σ_c are more sensitive to confining pressure and water content. The σ_{eb}/σ_c of carbonaceous slate decreases with an increase in the water content and confining pressure, which further validates the observation that the slate has much more acoustic emission events at the pre-peak stage when saturated and under high confining pressure.
4. The damage evolution process of carbonaceous slate can be divided into four stages: the initial damage phase (stage 1), the stable development of damage (stage 2), the damage acceleration and failure phase (stage 3), and the residual damage phase (stage 4). A new brittleness energy index *BDE* is proposed based on the damage evolution mechanism and the energy storage capacity of rock.

Acknowledgements This research was financially supported by the National Key R&D Program of China (Nos. 2016YFC0802201 and 2016YFC0802210) and Doctoral Innovation Fund Program of Southwest Jiaotong University.

Compliance with ethical standards

Conflict of interest The authors declare that we have no conflict of interest.

References

1. Aubertin M, Gill DE, Simon R (1994) On the use of the brittleness index modified (BIM) to estimate the post-peak behavior of rocks. Aqua Fennica 23:24–25
2. Bennett KC, Berla LA, Nix WD, Borja RI (2015) Instrumented nanoindentation and 3D mechanistic modeling of a shale at multiple scales. Acta Geotech 10(1):1–14
3. Cai M, Kaiser PK, Tasaka Y, Maejima T, Morioka H, Minami M (2004) Generalized crack initiation and crack damage stress thresholds of brittle rock masses near underground excavations. Int J Rock Mech Min Sci 41(5):833–847
4. Chen L, Liu JF, Wang CP, Liu J, Su R, Wang J (2014) Characterization of damage evolution in granite under compressive stress condition and its effect on permeability. Int J Rock Mech Min Sci 71(287–290):340–349

5. Deng Y, Chen M, Jin Y, Zou DW (2016) Theoretical analysis and experimental research on the energy dissipation of rock crushing based on fractal theory. J Nat Gas Sci Eng 33:231–239
6. Duan K, Kwok CY, Ma X (2016) DEM simulations of sandstone under true triaxial compressive tests. Acta Geotech 12:495–510
7. Eberhardt E, Stead D, Stimpson B, Read R (1998) Identifying crack initiation and propagation thresholds in brittle rock. Can Geotech J 35(2):222–233
8. Erguler ZA, Ulusay R (2009) Water-induced variations in mechanical properties of clay-bearing rocks. Int J Rock Mech Min Sci 46(46):355–370
9. Feng XT, Chen SL, Zhou H (2004) Real-time computerized tomography (CT) experiments on sandstone damage evolution during triaxial compression with chemical corrosion. Int J Rock Mech Min Sci 41(2):181–192
10. Fortin J, Stanchits S, Dresen G, Gueguen Y (2009) Acoustic emissions monitoring during inelastic deformation of porous sandstone: comparison of three modes of deformation. Pure Appl Geophys 166(5):823–841
11. Guo JQ, Liu XL, Qiao CS (2014) Experimental study of mechanical properties and energy mechanism of karst limestone under natural and saturated states. Chin J Rock Mech Eng 33(2):296–308
12. Hua AZ, You MQ (2001) Rock failure due to energy release during unloading and application to underground rock burst control. Tunn Undergr Sp Tech 16(3):241–246
13. Khazaei C, Hazzard J, Chalaturnyk R (2015) Damage quantification of intact rocks using acoustic emission energies recorded during uniaxial compression test and discrete element modeling. Comput Geotech 67:94–102
14. Kim JS, Lee KS, Cho WJ, Choi HJ, Cho GC (2015) A comparative evaluation of stress–strain and acoustic emission methods for quantitative damage assessments of brittle rock. Rock Mech Rock Eng 48(2):495–508
15. Li HR, Yang CH, Liu YG, Chen F, Ma HL, Wang BW (2014) Experimental research on ultrasonic velocity and acoustic emission properties of granite under failure process. Chin J Geotech Eng 36(10):1915–1923
16. Ma CC, Li TB, Xing HL, Zhang H, Wang MJ, Liu TY, Chen GQ, Chen ZQ (2016) Brittle rock modeling approach and its validation using excavation-induced micro-seismicity. Rock Mech Rock Eng 49(8):1–14
17. Martin CD, Chandler NA (1994) The progressive fracture of Lac du Bonnet granite. Int J Rock Mech Min Sci 31(6):643–659
18. Martin CD (1993) The strength of massive Lac du Bonnet granite around underground openings. Ph.D. thesis, University of Manitoba
19. Meng LB, Li TB, Jiang Y, Wang R, Li YR (2013) Characteristics and mechanisms of large deformation in the Zhegu mountain tunnel on the Sichuan-Tibet highway. Tunn Undergr Sp Tech 37(6):157–164
20. Mohamadi M, Wan RG (2016) Strength and post-peak response of Colorado shale at high pressure and temperature. Int J Rock Mech Min Sci 84:34–46
21. Nakao A, Nara Y, Kubo T (2016) P-wave propagation in dry rocks under controlled temperature and humidity. Int J Rock Mech Min Sci 86:157–165
22. Nara Y, Hiroyoshi N, Yoneda T, Kaneko K (2010) Effects of relative humidity and temperature on subcritical crack growth in igneous rock. Int J Rock Mech Min Sci 47(4):640–646
23. Nara Y, Morimoto K, Yoneda T, Hiroyoshi N, Kaneko K (2011) Effects of humidity and temperature on subcritical crack growth in sandstone. Int J Solids Struct 48(7–8):1130–1140
24. Peng RD, Ju Y, Gao F, Xie HP (2014) Energy analysis on damage of coal under cyclical triaxial loading and unloading conditions. Chin J Coal Sci Eng 39(2):245–252
25. Pestman BJ, Munster JGV (1996) An acoustic emission study of damage development and stress-memory effects in sandstone. Int J Rock Mech Min Sci 33(6):585–593
26. Schreyer H, Sulsky D (2016) Constitutive and numerical framework for modeling joints and faults in rock. Int J Num Analyt Meth Geomech 40(9):1253–1283
27. Semnani SJ, White JA, Borja RI (2016) Thermoplasticity and strain localization in transversely isotropic materials based on anisotropic critical state plasticity. Int J Num Analyt Meth Geomech 40(18):2423–2449
28. Tjioe M, Borja RI (2015) On the pore-scale mechanisms leading to brittle and ductile deformation behavior of crystalline rocks. Int J Num Analyt Meth Geomech 39(11):1165–1187
29. Tjioe M, Borja RI (2016) Pore-scale modeling of deformation and shear band bifurcation in porous crystalline rocks. Int J Numer Meth Engng 108(3):183–212
30. Wang SR, Liu ZW, Qu XH, Fang JB (2009) Large deformation mechanics mechanism and rigid-gap-flexible-layer supporting technology of soft rock tunnel. Chin J Highway Trans 22(6):90–95
31. Xie HP, Ju Y, Li LY, Peng RD (2008) Energy mechanism of deformation and failure of rock masses. Chin J Rock Mech Eng 27(9):1729–1739
32. Xie HP, Liu JF, Ju Y, Li J, Xie LZ (2011) Fractal property of spatial distribution of acoustic emissions during the failure process of bedded rock salt. Int J Rock Mech Min Sci 48(8):1344–1351
33. Xie HP, Peng RD, Ju Y (2004) Energy dissipation of rock deformation and fracture. Chin J Rock Mech Eng 23(21):3565–3570
34. Xiong DG, Zhao ZM, Su CD, Wang GY (2011) Experimental study of effect of water-saturated state on mechanical properties of rock on coal measure strata. Chin J Rock Mech Eng 30(5):998–1006
35. Yang SQ, Jing HW, Wang SY (2012) Experimental investigation on the strength, deformability, failure behavior and acoustic emission locations of red sandstone under triaxial compression. Rock Mech Rock Eng 45(4):583–606
36. Yang T, Xu T, Liu H, Zhang CM, Wang SY, Rui YQ, Shen L (2014) Rheological characteristics of weak rock mass and effects on the long-term stability of slopes. Rock Mech Rock Eng 47(6):2253–2263
37. Yu HC, Zhao Y, Liu HD (2015) Experimental study of influence of water on stress relaxation of rock under triaxial stresses. Chin J Rock Mech Eng 34(2):313–322
38. Zhou H, Meng FZ, Zhang CQ, Rongchao XU, Jingjing LU (2014) Quantitative evaluation of rock brittleness based on stress-strain curve. Chin J Rock Mech Eng 33(6):1114–1122
39. Zhang K, Cao P, Ma G, Wang WH, Fan WC, Li KH (2016) Strength, fragmentation and fractal properties of mixed flaws. Acta Geotech 11(4):901–912